SYSTEMATIC INVERSION OF RECEIVER FUNCTIONS & SURFACE-WAVE DISPERSION FOR CRUSTAL STRUCTURE IN CENTRAL ASIA

Charles J. Ammon,[1] George E. Randall,[2] Jordi Julia,[1] Robert B. Herrmann,[3] Eliana Arias[1]

Penn State University[1] Los Alamos National Laboratory,[2] and Saint Louis University[3]

Sponsored by National Nuclear Security Administration
Office of Nonproliferation Research and Engineering
Office of Defense Nuclear Nonproliferation

Contract No. DE-FC03-02SF22498[1,3] and W-7405-ENG-36[2]

ABSTRACT

We report on our initial investigations into the seismic structure of the lithosphere in central Asia using surface waves and receiver functions. We are relying on global and regional tomographic analyses for long-period surface-wave dispersion constraints on the structure, which we supplement with short-period observations measured directly from regional signals (when available). We plan to present an overview of receiver function complexity across the region using results from previous studies and receiver functions from many of the permanent stations. We will also present preliminary results from a small-scale short-period tomographic analysis of sparse observations across the Tibetan Plateau. The short period information is critical to tight constraints on shallow shear-wave velocity structure, but the measurements are sensitive to source location and origin time uncertainties. We will illustrate the combined inversion of surface-waves and receiver functions using a variety of model constraints. Our initial efforts will focus on permanent stations and temporary stations for which data are already in hand.

OBJECTIVES

Our objectives are the construction of shear-velocity profiles for regions surrounding broadband seismic stations throughout central Asia. Application of the technique in the region provides an opportunity to revise models of the crust and upper mantle structure throughout the region and to exploit the global and regional work of previous seismic verification research (*e.g.* Pasyanos *et al.*, 2001; Ritzwoller & Levshin, 1998, Larson and Ekstrom, 2001, Stevens and McLaughlin, 2001). The resulting shear-velocity models provide a single structure consistent with a range of observations and that can be tested as a tool for the construction of mode isolation filters that can help improve surface-wave magnitude estimates. We also plan to explore the possibility of adding data to our inversions of receiver functions, surface-wave dispersion. The diverse seismic activity throughout the region will facilitate cross-validation of the mode isolation filters with simple empirical filters constructed using larger events with adequate signal-to-noise ratios.

Background

Much of the background for this project is identical to that found in Simultaneous Inversion Of Receiver Functions, Multi-Mode Dispersion, And Travel-Time Tomography For Lithospheric Structure Beneath The Middle East And North Africa , by Ammon *et al.*, which appears elsewhere in these Proceedings. We refer the reader to this other work for general background information and use this space to provide more details on the inversion method and constraints that we have incorporated into the technique.

The Joint Inversion of Receiver Functions and Surface-Wave Dispersion Curves

The receiver function is sensitive to velocity transitions and vertical travel times. Surface-wave dispersion measurements are sensitive to averages of the velocities, and relatively insensitive to sharp velocity contrasts. The complementary nature of the signals makes them ideal selections for joint study because they can fill in resolution gaps of each data set. Ammon and Zandt (1993) pointed this out in a study of the Landers region of southern California (although for their specific case, available observations were unsuitable to resolve subtle features in the lower crust) and Ozalaybey *et al*. (1997) and Last *et al*. (1997) have performed complementary analyses of surface-wave dispersion and receiver functions and Du and Foulger (1999) implemented a joint inversion of these data types. The mechanics of the inversion are relatively simple since partial derivatives of dispersion observations (Herrmann, 1995) and receiver functions waveforms *(e.g*., Randall, 1989, Ammon *et. al*, 1990) can be calculated quickly and accurately.

The inversion is formulated to allow convenient adjustment of the relative importance of the different signals on the resulting models. We use an iterative least-squares approach to minimize a functional, *S(x),* which contains two terms corresponding to the two sets of observations (*N* receiver function sample points, y, and *M* dispersion observations, *z*) adjusted to an approximate unit variance. A control parameter, *p*, is used to adjust the importance of each set of observations.

$$\mathbf{S(x)} = \left\{ \frac{(1-\mathbf{p})}{\mathbf{N}} \cdot \sum_{\mathbf{i}=1}^{\mathbf{N}} \left(\frac{\mathbf{y_i} - \mathbf{A x_i}}{\sigma_{\mathbf{y_i}}} \right)^2 + \frac{\mathbf{p}}{\mathbf{M}} \cdot \sum_{\mathbf{i}=1}^{\mathbf{M}} \left(\frac{\mathbf{z_j} - \mathbf{B x_j}}{\sigma_{\mathbf{z_j}}} \right)^2 \right\} \tag{1}$$

No *a priori* approach is available to select an optimal weighting parameter, and the choice is made best after a systematic study of the inversions produced with a range of weights on each set of observations. At times the appropriate value of the trade-off parameter can be made by studying the fits. You may not want to fit part of a waveform that you know may be corrupted by off-azimuth arrivals, or you may not want to fit a rough portion of a noisy dispersion curve. These seismological decisions are not easily coded, but the decisions are easy after a careful study of the matches to the signals for a range of inversion weights. The overriding philosophy is simply to construct a model that suitably matches the observed dispersion and receiver functions.

Iterative "Jumping" Inversion Scheme. We use a jumping algorithm to jointly invert receiver functions and surface-wave observations for shear-wave velocity (Constable *et al.*, 1987). The jumping scheme allows us to implement a smoothness constraint in the inversion by minimizing a model roughness norm (Constable *et al.*, 1987; *Ammon et al.*, 1990) that can trade off with the prediction error. Our inversion weighting scheme accounts for the different num-

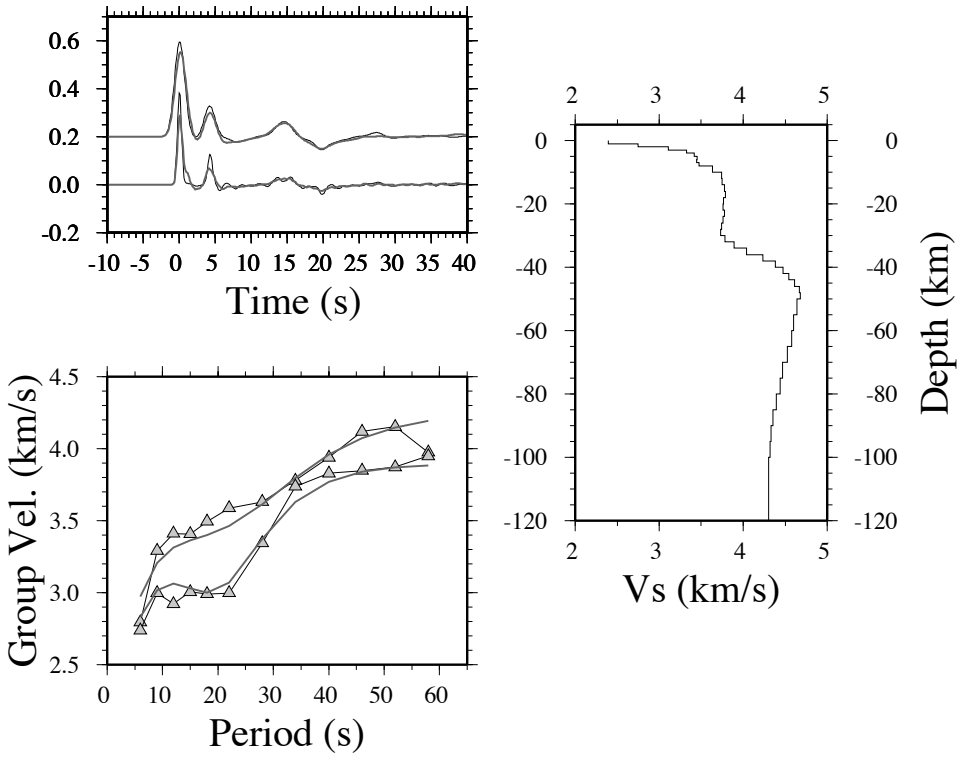

Figure 1. Observations, predictions, and shear-velocity model resulting from the joint inversion of receiver functions and fundamental-mode surface-wave dispersion measurements corresponding to station SODA located on the western Arabian Shield. The combination of the two data sets results in a simple crust with relatively smooth features but strong gradients despite the use of thin layers.

ber of data points and different physical units of each data set, and incorporates an *a priori* parameter that allows us to investigate the relative influence of each data set in the resulting models (Julia *et al.* 2000). Our model parameters are velocities of fixed-thickness layers overlying a half-space. The system of equations to be inverted is

$$\begin{bmatrix} \mathbf{pD_s} \\ \mathbf{qD_r} \\ \sigma\Delta \end{bmatrix} \cdot \mathbf{m} = \begin{bmatrix} \mathbf{pr_s} \\ \mathbf{qr_r} \\ 0 \end{bmatrix} + \begin{bmatrix} \mathbf{pD_s} \\ \mathbf{qD_r} \\ 0 \end{bmatrix} \cdot \mathbf{m}_0 \tag{2}$$

where $\mathbf{D_s}$ and $\mathbf{D_r}$ are the partial derivative matrices for the dispersion measurements and the receiver function estimates, respectively, $\mathbf{r_s}$ and $\mathbf{r_r}$ are the corresponding vectors of residuals, $\mathbf{m}$ is the vector of S-wave velocities, $\mathbf{m}_0$ is the starting model, and Δ is a matrix that constructs the second difference of the model. The partial derivative matrices and the vectors of residuals are normalized to equalize the different number of data points and physical units in the data sets. A number of trade-off parameters must be specified before inversion. The influence factor, $\mathbf{p}$, controls the trade-off between fitting receiver functions and dispersion curves, and the smoothness parameter, σ, controls the trade-off between data fitting and model smoothness. The parameter $\mathbf{q} = 1 - \mathbf{p}$, so that $\mathbf{p}$ is meaningless outside the range $0 \le \mathbf{p} \le 1$.

We begin with an example illustrating the inversion. Although the example data are not from Asia, they serve the present need to illustrate the value of constraints in the joint inversion. Figure 1 is a plot of the observed and predicted radial receiver functions and fundamental mode group velocity values for station SODA located near the western edge of the Arabian Shield. The receiver function sampled the structure into the Shield and away from the coast. The resulting shear-velocity profile is shown on the right. The shear-velocity model layers are 1 km thick for depths down

to 8 km, 2-km thick from 8- to 50-km depth, and 5 km thick from 50- to 100-km depth, beneath which is a uniform half-space. The trade-off parameters for the inversion, $\mathbf{p} = 0.4$ and $\sigma = 1.0$, were chosen empirically, after a systematic study of the inversion results produced for a range of values, as described in Julia *et al.* (2000). The starting model was a uniform 8.0 km/s P-wave velocity half-space. The resulting model is relatively simple, with a strong, shallow velocity gradient with a two-layer crust underlain by a transitional lower crust. The upper mantle is smooth, but contains a low-velocity zone below 50 km.

Although simple, this model poses some interpretational challenges. First the shallow structure appears to be too slow when compared with more detailed models of shallow shield structure that suggest an average velocity of 3.2 km/s for the top kilometer (Mokhtar *et al.,* 1988). Our surface low-velocity structure is 3 to 4 km thick, much more than the 400-m layer in higher-frequency studies. After considerable numerical experimentation, we found it necessary to omit the shortest periods for Love waves (T = 5 and 9 s) to remain consistent with geologic and seismic constraints on shallow structure of the Shield (e.g. Mokhtar *et al.*, 1988). We believe that the likely source of the problem is an overly smoothed tomography that produces slower than true group velocities in the shield, a result of compromising between the adjacent fast shield and slow platform on the western Arabian peninsula.

Also worth close inspection is the need for the decrease in velocity throughout the upper mantle in the model. The half-space velocity is significantly low for a shield, and a simple check of the long-period dispersion shows values that are much lower than those commonly observed. The model's deepest velocities are controlled by the long-period Rayleigh waves, and not surprisingly, since our longest period is 60 s, we cannot uniquely resolve much of the deeper structure in the model. However, although our observations cannot unambiguously constrain the deep structure, they are sensitive to deep features in the model, particularly an infinitely deep half-space located at such a shallow depth. Our concern is that the anomalous structure in the mantle may still trade off with features in the crust. To minimize the extent that deep velocity features may influence crustal features, we decided to constrain our results to transition smoothly into *a priori* mantle structures. Although we do not know *a priori* the deep structure, we are confident that PREM (Dziewonski and Anderson, 1980) or slight modifications from PREM velocities are certainly a better choice than an unconstrained component in our band-limited inversion. In practice we can implement constraints to be consistent with global aspherical shear velocity models since we need only know the values of deeper mantle shear velocity beneath the station (which we can get for the shear-wave models). Of course we could include longer-period tomographic dispersion measurements from other studies into our inversion to also help alleviate the problem.

Constraining The Solution

The upper mantle. The upper mantle low-velocity zone in Figure 2 may be a consequence of the limited resolving power at depth of our data set. To test the hypothesis, we incorporated *a priori* information to compel the deepest layers in our model to resemble values from global mantle models like S12WM13 (Su *et al.*, 1994). We chose to constrain our solution by appending the following set of equations to the original system (1) (Jackson, 1972),

$$\mathbf{W} \cdot \mathbf{m} = \mathbf{W} \cdot \mathbf{m}_{\mathbf{a\ priori}} \tag{3}$$

where $\mathbf{W}$ is a diagonal matrix of constraint weights and $\mathbf{m}_{\mathbf{a\ priori}}$ contains *a priori* predefined velocity values. We also thicken the model to move the half-space to a depth of 500 km, well below the depth of influence in our band width. The resulting models are satisfactory in that they predict dispersion values more consistent with global observations than do the truncated-depth models. The results of an inversion using a constrained upper mantle are shown in Figure 2. The constrained inversions incorporate *a priori* estimates of mantle velocities for depths greater than 100 km (down to 500 km), but prohibit the receiver function data to influence this part of the model. The starting model from the surface to 100-km depth and the parameters $\mathbf{p}$ and σ were identical to those used in the unconstrained inversion (Figure 2). The receiver functions for all the resulting models are essentially identical, and show good agreement with the data, and the predicted dispersion values are effectively identical up to 3-s period. The constraint still allows acceptable fits to our observations and insures that our models are close to those required by longer period surface-wave observations.

The shallow crust. Short-period ($\mathbf{T} < 10\mathbf{s}$) dispersion observations provide strong constraints on shallow shear-wave structure. The previous inversions have illustrated that a consequence of fitting the shortest period dispersion values

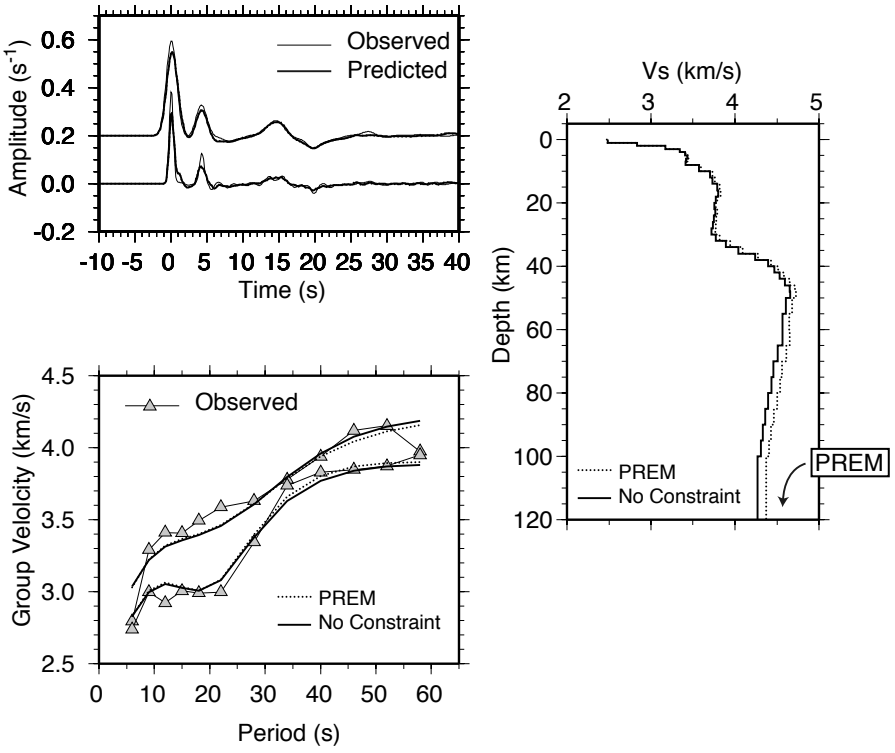

Figure 2. Results of the joint inversion of the receiver function and the intermediate-period Rayleigh group velocity values recorded near station SODA, Saudi Arabia (*p = 0.6*). The observed (solid line) and predicted (dashed line) receiver functions are shown in the upper left, the dispersion on the lower left, and the resulting shear velocity model on the right. The receiver functions were computed with Gaussian filter width factors of 1.0 and 2.5 to emphasize and exploit the frequency dependence of features in the response. The starting model was a uniform layered half-space.

from the tomographic models is unexpectedly slow velocities in the uppermost crust, inconsistent with the average 3.2 km/s that Mokhtar *et al.* (1988) inferred for the top kilometer from high-frequency (1-20 Hz) Rayleigh waves. Using thinner layers or an adaptive smoothness constraint near the surface did not alleviate the discrepancy, but numerical experiments suggested that the low velocities in our models were a consequence of the slow Love-wave group velocities for periods less than 10 seconds. Since these values are not well resolved by the tomographic study (Mokhtar*, et al.*, 2001) we repeated the inversion excluding the short-period (6 and 9 s) Love wave group velocities. Figure 3 is a comparison of the inversion results thus obtained with the full dispersion curve with an inversion excluding the 6-9 s period Love wave group velocities. We also increased the smoothing in the upper crust ($\sigma = 2.0$ for the upper 8 km, $\sigma = 1.0$ otherwise). The effects on the shallow crust are substantial, but the new results are more consistent with high-frequency Rayleigh dispersion analysis of Mokhtar *et al.* (1988) and with the geology of the Shield. The faster upper crust also improves the match to the peak P-wave amplitude on the broadband receiver function. As expected an increase in near-surface velocity deepens the shallowest velocity contrast, a clear example of the receiver function depth-velocity trade off (Ammon *et al.*, 1990), but the size of the upper crustal contrast is unchanged. Slight changes in the lower crust and upper mantle are noticeable.

RESEARCH ACCOMPLISHED

Receiver Function Computation

The first step in the project is the selection of target stations and the computation of receiver functions at those stations. To begin, we have selected a subset of permanent stations that have relatively long recording histories and thus will have substantial data already available. We plan to include all available temporary and permanent stations within the central Asian mainland. More recently installed stations and operating temporary stations will be added later in

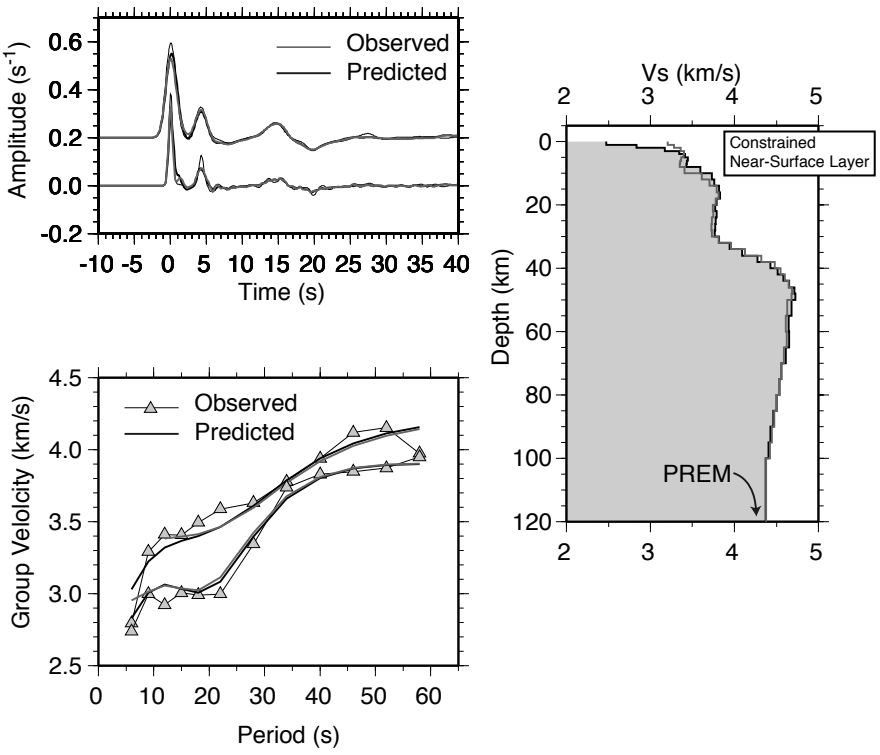

Figure 3. Inversion results with a requirement that the deep structure resemble an adjusted PREM (actually slightly modified to match Harvard Model SH12WM13 (Su *et al*., 1994) and that the shallow structure match to *a priori* information on near-surface velocities for the Shield. The constrained model produces a faster near surface layer at the expense of not fitting the shortest period Love wave dispersion from the tomography. The change in the upper crust shifts the mid-crustal boundary down about 2 km but does little else to the model.

the project. Data that we have begun to process at the time this report was written are shown in Figure 4. Example receiver functions for station BRVK in central Asia are shown in Figure 5. Receiver functions generally vary with azimuth and ray parameter and so we summarize our observations in two profiles to show the variation with each. As a first order approximation of the structure, we ve ignored azimuthal variation and performed a stacking procedure to use the waveforms to estimate the thickness and Poisson s ratio of the crust (assuming that Vp ~ 6.2 km/s) using the method of Zhu and Kanamori (2000). The resulting fits are reasonable, with a thickness value of about 45 km and a Poisson s ratio of 0.26. We will perform similar analyses and inversions for each station with suitable data. When necessary (or possible), we will split the data as a function of azimuth to produce estimates of the lateral heterogeneity associated with each site.

CONCLUSIONS AND RECOMMENDATIONS

Since we have just begun work in this project in the last few months, conclusions and recommendations are premature.

ACKNOWLEDGEMENTS

We thank P. Wessel and W. H. F. Smith, the authors of GMT for producing easy-to-use, quality software for making maps and charts.

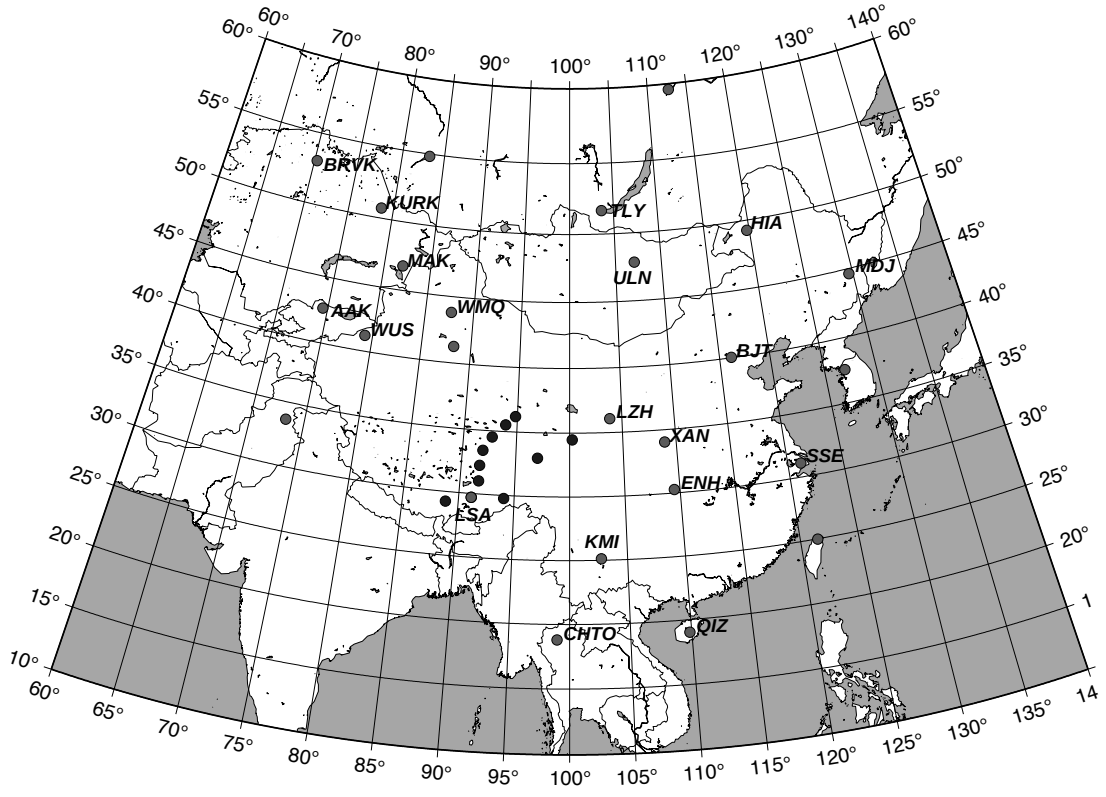

Figure 4. Open stations that we have targeted for analysis as part of this project. The stations are located in a range of environments, and most have some regional activity nearby that we can use to add short-period dispersion measurements and to test the resulting shear-velocity models.

REFERENCES

Ammon, C.J., G.E. Randall, and G. Zandt (1990), On the non-uniqueness of receiver function inversions, *J. Geophys. Res.*, **95**, 15303-15318.

Ammon, C. J., and G. Zandt (1993), The receiver structure beneath the southern Mojave Block, *Bull. Seism. Soc. Am.*, **83**, 737-755.

Constable, S.C., R.L. Parker, and C.G. Constable (1987), Occam's inversion: A practical algorithm for generating smooth models from electromagnetic sounding data, *Geophysics*, **52**, 289-300.

Du, Z.J. and G.R. Foulger (1999), The crustal structure beneath the northwest fjords, Iceland, from receiver functions and surface waves, *Geophys. J. Int.*, **139**, 419-432.

Dziewonski, A.M., and D.L. Anderson (1981), Preliminary reference Earth model, *Phys. Earth Planet. Int.*, **25**, 297-356.

Herrmann, R. B., *Computer Programs in Seismology, 1995*, Saint Louis University, St. Louis, MO, USA.

Jackson, D.D., Interpretation of inaccurate, insufficient, and inconsistent data (1972), *Geophys. J. R. Astron. Soc.*, **28**, 97-109.

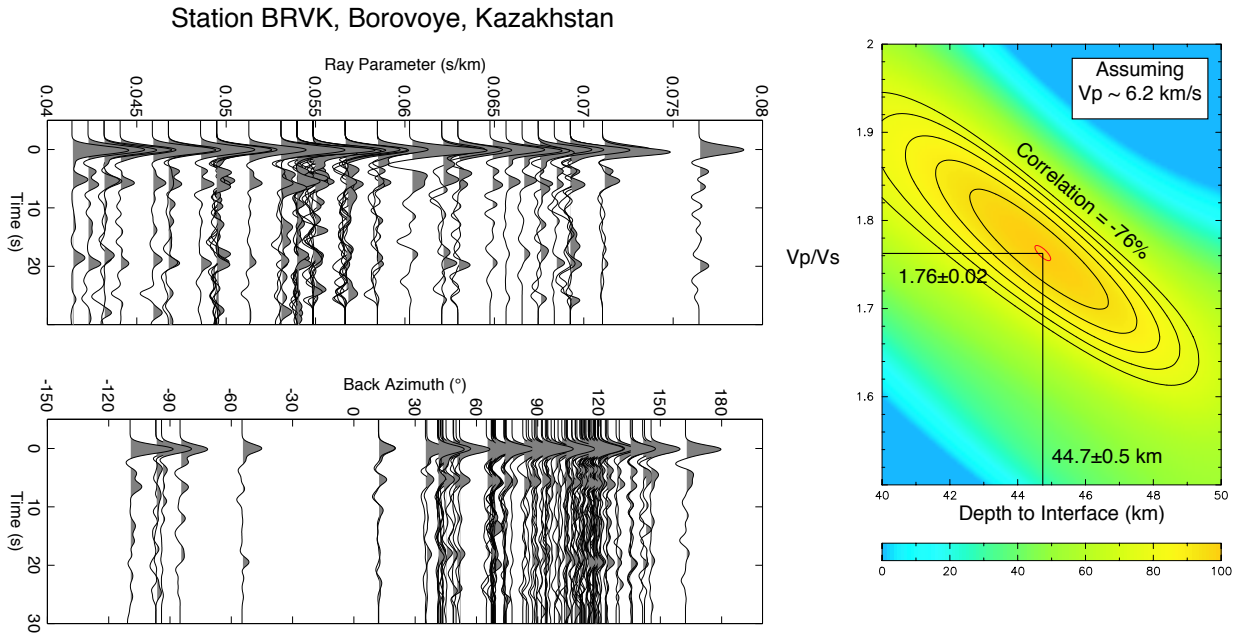

Figure 5. Sample receiver function observations and a limited analysis of Poisson's ratio and crustal thickness (assuming Vp ~ 6.2 km/s). The observed receiver functions are shown as a function of ray parameters (sin of the P-wave incident angle) and as a function of back azimuth. The data do not sample the azimuthal structure uniformly as teleseisms are predominantly observed from western Pacific subduction zones. The ray parameter sampling is good, and identifiable conversions and multiples are seen clearly for a range of incident angles. The image on the right shows the results of stacking all waveforms to identify the crust-mantle transition. Uncertainties were estimated using a jack-knifing technique. These uncertainties are conservative since they also depend on the assumed P-velocity of the crust. As a result of azimuthal sampling, the results are most reflective of the structure to the east of the station.

Julia, J., C. J. Ammon, R. B. Herrmann, and A. M. Correig (2000), Joint Inversion of receiver function and surface-wave dispersion observations, *Geophys. J. Int.* **143**, 99-112.

Larson, E. W. F. and G. Ekstr m (2001), Global Models of Group Velocity, *Pure and Applied Geophys.*, **158**, 1377-1399.

Last, R. J., A. A. Nyblade, C. A. Langston and T. J. Owens (1997), Crustal structure of the East African Plateau from receiver functions and Rayleigh wave phase velocities, *J. Geophys. Res.*, 102, 24,469-24,483.

Mokhtar, T. A., R. B. Herrmann, and D. R. Russell (1988), Seismic velocity and Q model for the shallow structure of the Arabian shield from short-period Rayleigh waves, *Geophysics*, **53**, 1379-1387.

Mokhtar, T. A., C. J. Ammon, R. B. Herrmann (2001), and H. A. A. Ghalib, Lithospheric structure beneath Arabia, *Pure and Applied Geophys*, **158**, 1445-1474.

Nalaybey, S., M.K. Savage, A.F. Sheehan, J.N. Louie, and J.N. Brune (1997), Shear-wave velocity structure in the northern Basin and Range Province from the combined analysis of receiver functions and surface waves, *Bull. Seismol. Soc. Am.*, **87**, 183-199.

Pasyanos, M.E., W.R. Walter, and S.E. Hazler (2001), A Surface wave dispersion study of the Middle East and North Africa for Monitoring the Comprehensive Nuclear-Test-Ban Treaty, *Pure and Applied Geophys*, **158**, 1445-1474.

Randall, G. E. (1989), Efficient calculation of differential seismograms for lithospheric receiver functions, *Geophys. J. Int.*, **99**, 469-481.

Ritzwoller, M. H. and A. L. Levshin (1998), Eurasian surface wave tomography: Group velocities, *J. Geophys. Res.,* **103**, 1839-1878.

Stevens, J. L. and K. L. McLaughlin (2001), Optimization of Surface Wave Identification and Measurement, *Pure and Applied Geophys*., **158**, 1547-1582

Su, W., R. L. Woodward, and A. M. Dziewonski (1994), Degree 12 model of shear velocity heterogeneity in the mantle, *Nature*, **99**, 6945-6980.

Zhu, L., and H. Kanamori (2000), Moho depth variation in Southern California from teleseismic receiver functions, *J. Geophys. Res.*, **105** (2), 2969-2980.